Thick thermoplastic composite laminate consolidation: Experimental observations and numerical approaches

Yvan Denis, Tuan-Linh Nguyen, Damien Lecointe, Steven Le Corre, Arthur Lévy

Journal Title
XX(X):2–35

DOI: 10.1177/ToBeAssigned
www.sagepub.com/
SAGE

Thick thermoplastic composite laminate consolidation: experimental observations and numerical approaches

Yvan Denis [1], Tuan-Linh NGuyen [1], Damien Lecointe [1], Steven Le Corre [1], Arthur Levy [1]

Abstract

Since the benefits of composite materials have been demonstrated, particularly those relevant to the fields of transports and energy, increasingly high industrial expectations are emerging. As the control of the processes is complex, the thickness of the composite materials does not usually exceed a few millimetres. The aim of the work presented in this paper is to highlight new phenomena related to the oven/autoclave consolidation of thicker thermoplastic composites. In the case of such thick composites, the influence of certain phenomena that are usually neglected becomes important and a physical interpretation becomes necessary (the thermal contact resistance between mold and part and the influence of mold geometry). Here, an experimental approach is compared with numerical simulations of heat transfer and crystallization in order to validate the proposed thermokinetics model. Finally, some numerical observations are discussed and analyzed.

Keywords

thermoplastic composites, thermal contact resistance, numerical simulations, thick parts, composite manufacturing

Prepared using sagej.cls *[Version: 2017/01/17 v1.20]*

Introduction

The popularity of composite materials is generating new challenges for both experimental and numerical studies. The excellent ratio of mechanical characteristics to weight is leading manufacturers to seek increasing expertise with this type of material. The objective of this paper is thus to respond to a rather recent but very common problem in the transport and energy industry, which concerns the forming of high thickness composite parts. Often, 3D woven fabrics are used for manufacturing thick parts[1–3]. Indeed, until now, the thickness of the majority of manufactured composite parts has been only a few millimetres at the most. Nonetheless, some heavily loaded structural parts such as landing gears[4] or helicopter rotor hubs[5] require the manufacturing of very thick laminates. Manufacturing a thick thermoset matrix composite part appears very challenging. Among the main difficulties are the need to limit the exotherm effect and the overheating of the core, which requires a very long cycle with slow ramps[6–10]. Using thermoplastic matrices appears to offer a promising alternative solution to thermoset matrix composites because they require much lower transformation energy and can be processed with faster cycles.

In the literature, it has been shown that thicker parts are very sensitive to geometry, manufacturing conditions, and the multi-physical effects induced by this type of parts. Strong relationships between thermal, crystallisation or polymerisation chemistry as well as mechanics occur and can no longer be neglected.[10–16]. Several observations have shown the link between final part quality and process conditions. This link is much more sensitive for thicker parts than for thinner ones.[5,17–20]. Recently, an experimental approach has shown a strong causal link between local material health and the type of part being consolidated[18]. The geometry of the tooling in vacuum bag consolidation can create delaminations or crackings in

[1]Nantes Université, CNRS, Laboratoire de thermique et énergie de Nantes, LTeN, UMR 6607, IRT Jules Verne, F-44000 Nantes, France

Corresponding author:
Arthur Levy, Laboratoire de Thermique et Energie de Nantes, Nantes Université, 44000 Nantes Cedex, France.
Email: arthur.levy@univ-nantes.fr

Prepared using sagej.cls

very localised areas of the part. However, there is a lack of numerical models to understand the local evolution of stress, strain and material health.

The main objectives of this paper are to discuss some novel considerations and highlight some major issues in the thermal control of forming a high thickness composite part based on a fine-scaled 3D coupled thermal and crystallization model. The study and results presented below essentially target the consolidation phase, in an oven or autoclave, of a thermoplastic part previously draped by the automated fibre placement (AFP) process.

The complete thermal history of the material is, therefore, not taken into account in the present work. Its modelling assumptions are presented in the first part of this paper. Particular attention is paid to the shape of the temperature gradient through the thickness of the part and to the boundary conditions which can no longer be modelled by considering the usual simulation assumptions. Indeed, the thermal contact resistance is usually considered as either constant or negligible for thin parts[21–29] or thermoset composites[30–34]. The influence of the mold geometry and thermal effect are also commonly neglected. Moreover, when a thermoplastic part is of high thickness, it can potentially deform significantly due to anisotropic shrinkages created by the strongly heterogeneous temperature distribution and the phase transition of the resin during crystallization. Both of these types of associated shrinkage are already taken into account for thin material[15,35–43]. It was shown that the temperature field and thus the crystallization field are very sensitive to the thermal contact resistance (TCR). During the cooling in the consolidation process, deformation of the part, enhanced by thermal gradients, can create a contact loss between the surface of the part and the mold surface. Although TCR is classically considered as an adjustable parameter in the models, fine and representative physical models of TCR need to be employed for an accurate predictability of simulation tools. One should therefore refer to studies that examine this topic from a more physical angle, such as Kaminski et al.[44] or, for other applications, Domingues et al.[45] or Some et al.[46,47].

As experimental testing is often long and expensive, numerical approaches are of growing interest and provide indications for the

understanding and control of forming processes. Cost considerations are particularly relevant to thick high-performance composites used in aeronautics. In particular, in the case of thick composite materials, these approaches can help analyze the quality of parts (porosities, deformations, residual stresses, delamination, etc.). This article is composed of four parts, starting with the assumptions and properties of the models (section *Coupled heat transfer and crystallization model*). The next part (section *Experimental observations and comparisons with simulations*) concerns the experimental observations and model validation done by a comparison of the temperature gradient between a thin and a thick plate. This analysis is followed by a discussion on the influence of the thermal contact resistance and on the importance of taking this aspect into account. The last section (section *Numerical analysis*) complements the experimental observations with a numerical study on the influence of mold design on heat flow and its thermo-mechanical consequences.

In this paper, the consolidation of a commercial Carbon-PEEK layup of 65 to 192 plies laminate is considered. For this composite system, the material properties are available in the literature. In addition, the methodology was applied to the specific confidential carbon-PAEK system used in the industrial project. In the first section, the consolidation step, post-AFP, under vacuum is modelled using a coupled heat transfer and crystallization kinetics simulation. In the second section, the predicted temperatures are compared to experimental measurements using thermocouples. The model is thus validated. In the last section, the predictive model is used to discuss the effect of processing conditions on the final part homogeneity and quality.

Coupled heat transfer and crystallization model

The reheating/cooling phase of the manufacturing of a thick aerospace-grade carbon fibre thermoplastic composite (CFTP) part needs to be considered. This is often referred to as the *consolidation phase*. In this section, we will model the heat transfer and crystallization kinetics. The modelling set-ups, material properties and modelling assumptions will first be presented. The latter are

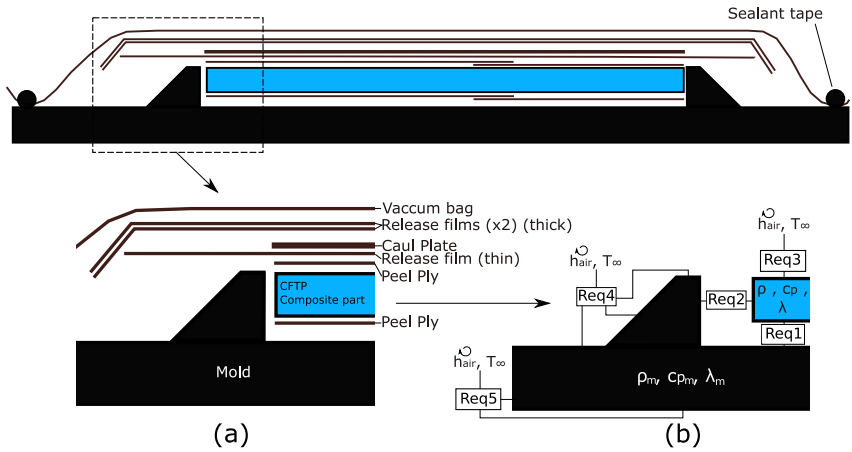

Figure 1. Experimental set-up. (a) details of the bagging system, (b) modelling strategies to consider each layer and each boundary condition using equivalent thermal contact resistances.

necessary to have a first adapted, manipulable and coherent numerical approach. These hypotheses are detailed below.

Main modelling assumptions

Two major assumptions are first adopted that make it possible to develop a simplified model that will be able to reasonably predict the temperature and crystallization fields.

- (i): Due to the large number of plies considered here (65 to 192) and the quite large in-plane dimensions, a full 3D study at the ply scale would be unaffordable and useless. The parts are draped according to an AFP lay-up sequence leading to a quasi-isotropic planar orientation. Subsequently, the composite part will be considered as a homogeneous transversely isotropic material (transverse direction along $\boldsymbol{z}$ in Fig. 1).
- (ii): This work focuses on the consolidation step after AFP. Once fully molten, during the dwell, the state of the part is supposed to be perfect, without porosities or defects. Due to the AFP process, the parts may exhibit defects, such as gaps or overlap between layers or delamination. The drastic thermo-mechanical conditions of this process are also likely to induce crystallization gradients and high residual stresses. It should be noted that this

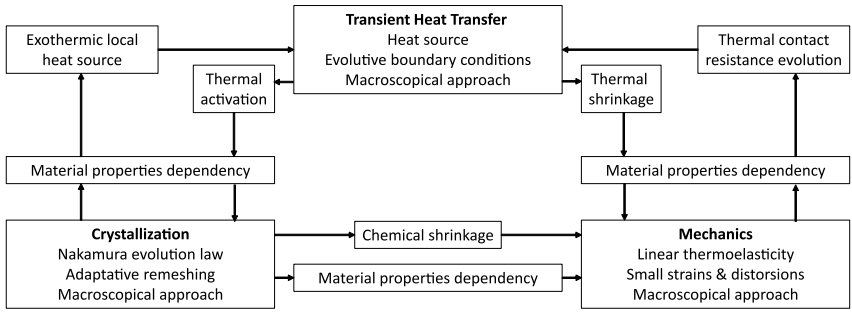

Figure 2. Linking the three physical processes to model the oven/autoclave consolidation process.

aspect is not taken into account in this work, which focuses on oven consolidation and its influence on the whole manufacturing line.

During the oven consolidation process, different physical processes are involved, such as heat transfer, crystallization and mechanics. Each of these is linked to the others by different phenomena, which makes simulations complex. Fig. 2 shows the connections between each physical process. Heat transfer is the first step of the process, which directly governs melting and then cooling and crystallization of the composite. It also controls the thermo-mechanics through thermal shrinkage and evolution of material properties. Indirectly, through the crystallization process, it also governs the so-called chemical shrinkage and the evolution of mechanical properties due to this transformation.

In order to simulate the main phenomena in the consolidation process of thick parts, the numerical approach developed here follows this guiding idea of linked processes, but focuses on a model including heat transfer and crystallization kinetics only. This will nevertheless enable discussion of the consequences for the consolidation process and the creation of residual stress and associated geometrical distortions.

The following modelling assumptions are adopted:

- (iii): Nakamura's model[48] is adopted for the crystallization kinetics.

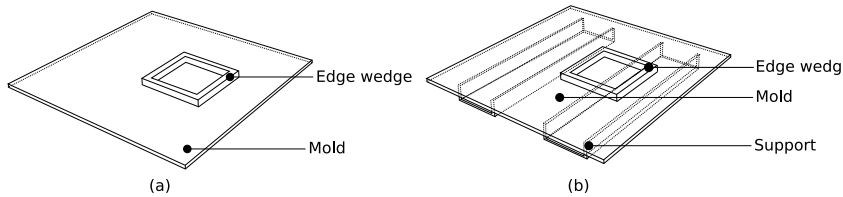

Figure 3. Experimental and numerical set-ups to compare the influence of thickness and mold geometry.

- (iv): The crystallization field is only calculated during the cooling phase. This will be called either crystallization field or α field in the rest of this paper.

Set-ups

To be able to compare the influence of either the thickness and/or the mold geometry on the thermal field, two representative lab-scale flat consolidation tooling set-ups were devised, as shown in Fig. 3.

As can be seen in the figure, set-up (a) is a simple steel (S235) plate with edge wedges to properly consolidate the CFTP part. Set-up (b) is the same, but with supports (e.g. for handling). The composite part is intentionally positioned above the support in order to observe its potential influences on the temperature field. The CFTP parts are considered as two 250 x 250 (mm x mm) size length plates.

Properties and material

The material used in this paper is a layup of 65 to 192 T300 J PEEK/Carbon prepreg plies. This 5 harness satin thermoplastic composite plies are made of 58% carbon fibre and 42% a PEEK matrix whose parameters are available in the literature, such as in the work of Tardif et al.[49], Landry and Hubert[50] or those using a PEEK material[51–54].

In addition, other simulations were done using a confidential PAEK thermoplastic composite system. Its parameters were obtained only by adjusting the descriptions of the matrix but without modifying the model presented hereunder.

Main modelling strategies

The entire thermokinetics solution was developed in the FreeFem++ library[55]. This FEM library has the advantage of being free and open source, which offers the user the possibility to develop specific and adapted algorithms. Indeed, here in this paper it is shown that thermal contact resistance (TCR) is of major importance for thick composite parts. Thermal contact resistance consists in quantifying the heat transfer between two domains (for example the part and the mold) by intrinsically taking into account surface defects, possible air gaps or contact losses[56–58]. FreeFem++ makes it possibile to properly consider this parameter by simultaneously solving the transient heat transfer both in the mold and in the part, thus introducing a strong coupling between domains. TCRs are usually supposed to be constant, both temporally and spatially, since the heat transfer in thin plates is mainly driven by convection and by conduction in the composite. This paper, on the contrary, shows that TCR has an important influence on the thermal field. Thus, a time and space dependency is considered such that:

$$TCR = TCR(x, y, z, t) \tag{1}$$

The simulation tool is based on the transient heat transfer modelling, usually written through the standard heat equation:

$$\rho(T, \alpha) c_p(T, \alpha) \frac{dT}{dt} - \boldsymbol{\nabla} \cdot (\boldsymbol{\lambda}(T, \alpha) \boldsymbol{\nabla}(T)) - r = 0 \tag{2}$$

where the following notations and material properties are introduced:

- T, temperature field, spatial and time dependant, such that $T = T(x, y, z, t)$ in Kelvin K.
- ρ, density, in $kg.m^{-3}$, is an conservative quantity and follows the rule of mixture:

$$\rho(T, \alpha) = \rho_{fibre} \Phi_\nu + (\alpha \cdot \rho_{amorph}(T) + (1 - \alpha) \cdot \rho_{cryst}(T)) (1 - \Phi_\nu) . \tag{3}$$

  where Φ_{nu} is the fibre volume fraction and α is assumed to equate the crystalline volume fraction. The values of the amorphous ρ_{amorph} and crystalline ρ_{cryst} densities of the matrix as well as the fibre density ϕ_{fibre} are taken from the literature and listed in Table 1 along with their sources.

- c_p, the specific heat, in $J.kg^{-1}.K^{-1}$ also follows the rule of mixture:

$$c_p(T) = c_{p,fibre}(T)\Phi_\nu + c_{p,resin}(T)\,(1-\Phi_\nu) \tag{4}$$

  where $c_{p,resin}$ and $c_{p,fibre}$ are given in Table 1.
- $\boldsymbol{\lambda}$, the conductivity tensor, is considered isotropic transverse because the layup is a quasi-iso. It is in $W.m^{-1}.K^{-1}$ and such that:

$$\boldsymbol{\lambda}\,(T,\alpha) = \lambda_{plane}\,(T,\alpha)\cdot(\overline{e}_x\otimes\overline{e}_x + \overline{e}_y\otimes\overline{e}_y) + \lambda_{thickness}\,(T,\alpha)\,\overline{e}_z\otimes\overline{e}_z \tag{5}$$

  assuming that $\boldsymbol{x}$ and $\boldsymbol{y}$ describe the in-plane directions and $\boldsymbol{z}$ the though thickness direction. $\otimes$ stands for the tensorial product. The effective composite conductivities λ_{plane} and $\lambda_{thickness}$ are assumed to follow the rule of mixture versus degree of crystallinity:

$$\begin{cases} \lambda_{plane}\,(T,\alpha) = \alpha\cdot\lambda^{amorph}_{plane} + (1-\alpha)\cdot\lambda^{cryst}_{plane}(T) \\ \lambda_{thickness}\,(T,\alpha) = \alpha\cdot\lambda^{amorph}_{thickness} + (1-\alpha)\cdot\lambda^{cryst}_{thickness}(T) \end{cases} \tag{6}$$

- $\boldsymbol{\nabla}$ is the spatial gradient operator.
- r is a source term accounting for the heat release due to crystallization, as discussed below.

The transient heat transfer modelling requires the following discretization:

- (i): A standard Euler iterative time integration scheme is adopted. The temporal domain thus decomposes time into increments. Contrary to what can happen for thin composite parts, thick composite parts induce a steep thermal gradient through the thickness. To be able to model the entire history of the material, simulations are performed for both the heating and the cooling phases of the thermal cycle.
- (ii): However, the spatial domain also remains very important. As can be seen in Fig. 1 (a) many layers are needed to follow the consolidation procedure. In order to be able to move toward realistic modelling, all the environment layers used for consolidation are taken into account (see Fig. 1), such as the

Table 1. Material properties used in the simulation

Property	Symbol	Value	Source
		Density $[kg/m^3]$	
Fibre	ρ_{fibre}	1770	59
Matrix			
- amorphous	$\rho_{amorphous}$	$1356.3 - 0.74 \cdot (T - 273.15)$	60
- crystalline	ρ_{cryst}	$\begin{cases} 1318.7 - 0.15 \cdot (T - 273.15) \\ \quad if \quad T \leq 423.15(K) \\ 1392.7 - 0.64 \cdot (T - 273.15) \\ \quad if \quad T > 423.15(K) \end{cases}$	51,54
		Fibre volume fraction $\Phi_\nu = 0.58$	50
		Heat Capacity $[J/m^3/K]$	
Fibre	$c_{p,fibre}$	$624.4 + 3.196 \cdot (T - 273.15)^2$	60
Matrix	$c_{p,resin}$	$953.4 + 3.103 \cdot (T - 273.15)$	60
		Thermal conductivity $[W.m^{-1}.K^{-1}]$	
In-plane			
- amorphous	λ_{plane}^{amorph}	5.92	60
- crystallized	λ_{plane}^{cryst}	$3.917 + 5 \times 10^{-3} \times (T - 273.15)$	60
Transverse			
- amorpous	$\lambda_{thickness}^{amorph}$	0.679	60
- crystallized	$\lambda_{thickness}^{cryst}$	$0.5615 + 1.7 \times 10^{-3} \times (T - 273.15)$	60

peel-plies, the caul-plate, etc. These layers are then numerically modelled with equivalent TCR. An initial gap between the mold and the part is also taken into account, following the work of Castell et al.[61]. Fig. 1 (b) presents the set of boundary conditions though a simplified representation of the experimental set-up.

The modelling also needs boundary conditions (BCs). Boundary conditions of the third type are considered[62]:

$$\begin{cases} \overline{\nabla}(T) \cdot \overline{n}_i = \frac{1}{Req_i} \cdot (T_{CFTP} - T_m) \quad \text{for} \quad i \in [1,2] \\ \overline{\nabla}(T) \cdot \overline{n}_i = \frac{1}{Req_i} \cdot (T_m - T_{CFTP}) \quad \text{for} \quad i \in [1,2] \\ \overline{\nabla}(T) \cdot \overline{n}_3 = \frac{1}{Req_3} \cdot (T_{CFTP} - T_\infty) \\ \overline{\nabla}(T) \cdot \overline{n}_i = \frac{1}{Req_i} \cdot (T_m - T_\infty) \quad \text{for} \quad i \in [4,5] \end{cases} \tag{7}$$

where n_i is the normal of the surface i of the composite part or the mold. Indexes m and $CFTP$ are related to the mold and the composite part, respectively. For a thick composite part, the BCs are of major importance. They must be correctly described in order to take into account every parameter of each phenomenon needed to carry out consolidation. The description of the BCs is therefore proposed below according to their position[63–67].

Table 2. Physical parameters for the boundary conditions of the numerical transient heat transfer model. *: Even if TCR1 (between the part and the mold associated with R_{eq1}) and TCR2 (between the part and the mold on the edges associated with R_{eq2}) are both dependant on time and space, an initial value is given. It is likely to be updated if there is contact loss. Kaminski's work[44] makes it possible to model an air gap (created by the contact loss) as a function of its thickness, temperature and pressure.

	Parameter	Description	Value	Unit
Thickness (e)	e_{pp}	pp: peel-ply	5.10^{-5}	m
	e_{rf}	rf: release film	5.10^{-5}	m
	e_{cp}	cp: caul-plate	0.02	m
	e_{vb}	vb: vacuum bag	5.10^{-5}	m
Conductivity (λ)	λ_{pp}	pp: peel-ply	0.05	$W.m^{-1}.K^{-1}$
	λ_{rf}	rf: release film	0.05	$W.m^{-1}.K^{-1}$
	λ_{S235}	cp: caul-plate	54	$W.m^{-1}.K^{-1}$
	λ_{vb}	vb: vacuum bag	0.05	$W.m^{-1}.K^{-1}$
TCR*	TCR_1	-	1.10^{-3}	$W^{-1}.m^2.K$
	TCR_2	-	1.10^{-3}	$W^{-1}.m^2.K$
Convection (h)	h_{air}	Forced convection	20	$W.m^{-2}.K^{-1}$

$$\begin{cases} Req_1 = \frac{e_{pp}}{\lambda_{pp}} + TCR_1 \\ Req_2 = TCR_2 \\ Req_3 = \frac{1}{h_{air}} + \frac{e_{pp}}{\lambda_{pp}} + 2\frac{e_{rf}}{\lambda_{rf}} + \frac{e_{cp}}{\lambda_{S235}} + \frac{e_{pp}}{\lambda_{pp}} + \frac{e_{vb}}{\lambda_{vb}} \\ Req_4 = \frac{1}{h_{air}} + \frac{e_{rf}}{\lambda_{rf}} + 2\frac{e_{pp}}{\lambda_{pp}} + \frac{e_{vb}}{\lambda_{vb}} \\ Req_5 = \frac{1}{h_{air}} \end{cases} \tag{8}$$

All of these equivalent resistances require material parameters; these are listed in Table 2:

In Fig. 1, the parameters ρ, c_p and $\boldsymbol{\lambda}$ are associated with the composite part by the index $CFTP$ and the mold by m. Thus, two equations of transient heat transfer are calculated. Written under weak formulation, it is possible to describe the matrix K of the problem useful for the implicit time integration solving strategy as follows:

$$[K]\,\overline{U} = \overline{F} \equiv \begin{bmatrix} K_m & K_{m,CFTP} \\ K_{CFTP,m} & K_{CFTP} \end{bmatrix} \begin{pmatrix} T_m \\ T_{CFTP} \end{pmatrix} = \begin{pmatrix} F_m \\ F_{CFTP} \end{pmatrix} \tag{9}$$

This formulation, from an implicit solver, enables the solving of the thermal field in the mold but also, simultaneously, in the composite

part. No iterations are required at each time step. The associated conditions of this solver and the guidelines to write the model under a weak formulation are presented in chapter 2.17, pages 75-77, of the FreeFem documentation[68]. Moreover, two main methods are available in FreeFem++ to solve the problem numerically: GMRES (for Generalized Method RESidual Method) or the Galerkin Sparsesolver.

The source term r in Eq. (2) accounts for the exotherm due to crystallization. This parameter makes the thermokinectic coupling. This term is classically defined as follows:

$$r = L \cdot f_{nak} = L \cdot \frac{d\alpha}{dt} \tag{10}$$

where L is the latent heat of crystallization of the composite and α is the degree of crystallization, ranging between 0 (fully molten) and 1 (fully crystallized up to the maximum value of the material). It is then possible to obtain the link between the transient thermic and the crystallization. Indeed, to update r, it is necessary to take into account the crystallization kinetics. To model such physical processes, there are several alternatives[69–71]. The one selected here for the numerical simulation is the Nakamura description[48,72,73]. The differential form of this model is described as follows using Levy's numerically robust strategy[73]:

$$\begin{cases} \frac{d\alpha}{dt} = K(T) \cdot n(1-\alpha) \cdot (-\ln(1-\alpha))^{\left(1-\frac{1}{n}\right)} & if \quad \alpha \leq \alpha_{max} \\ \frac{d\alpha}{dt} = K(T) \cdot n \cdot (1-\alpha) \cdot (-\ln(1-\alpha_{max}))^{\left(1-\frac{1}{n}\right)} & if \quad \alpha > \alpha_{max} \end{cases} \tag{11}$$

This equation requires some variables, which are defined below:

- $K(T)$ is the Nakamura kinetic function from Avrami's work[69] and is often described by an exponential function such that:

$$K(T) = \left(e^{-2.75e^{-3} \cdot T^3 + 2.818 \cdot T + -719.26}\right)^{\frac{1}{n}} \tag{12}$$

  with the parameters identified from a differential scanning calorimetry (DSC) experiment[74].
- n is the Nakamura index such that $n \in [1, 4]$. Here, $n = 3$[74], which corresponds to spherolitic (three dimensional) crystal growth with instantaneous germination.

Table 3. Temperature cycle applied during the oven consolidation process.

Time (h)	Temperature (°C)	Rate (°C)
0 (heating: t_h)	20	6
1.2 (waiting)	430	0
1.4 (cooling: t_c)	430	-2
5 (end)	20	0

- α_{max} is a numerical threshold defined in Levy[73] such that $\alpha_{max} = 0.98$.

In the finite element implementation, α is a scalar field. Thus, Eq. (11) is a local ordinary differential equation that has to be solved at each node.

The nonlinear differential Nakamura kinetics Eq.(11) is written:

$$\frac{d\alpha}{dt} = f_{nak}\left(\alpha_t, T_t\right) \tag{13}$$

and is solved by using a Newton-Raphson algorithm[75]. Eq. (13) can also be written as follows, at a given time t:

$$\alpha_t - \alpha_{t-1} - dt \cdot f_{nak}\left(\alpha_t, T_t\right) = 0 \tag{14}$$

Experimental observations and comparisons with simulations

subsectionInstrumentation

The objective of this section is to compare the main numerical results from the models presented above with experimental observations. To do this, set-up B was used to consolidate two plates, one thin/medium (12 mm thick) and one thicker (35 mm thick) (see Fig. 4). These two plates were instrumented with thermocouples. The temperature is considered homogeneous inside the oven and follows the cycle described in Table 3.

Sixteen type K thermocouples were made with 125 micron diameter chromel and alumel wires by goodfellow coated with polyimide varnish. 3 mm thick laminates were layed by AFP and stacked to add up to a 12 mm (9 mm thick laminates stacked to add up to 35 mm) thick laminates. This allowed for the positioning of thermocouples as described in Fig. 4 and Table 4. Note that this positioning between

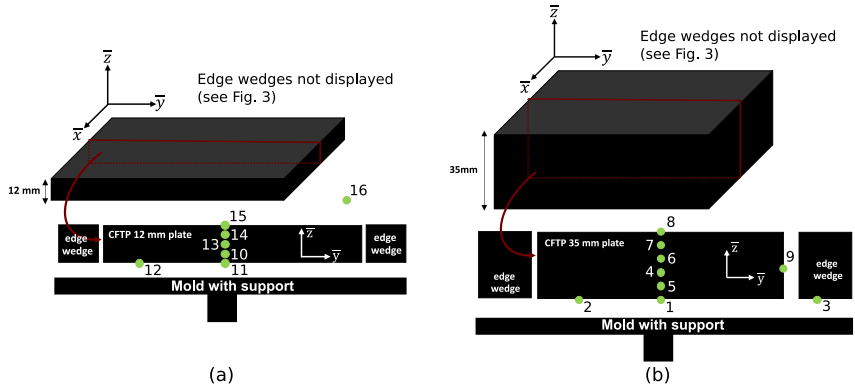

Figure 4. Experimental set-up and locations of the 16 thermocouples positioned inside and outside the composite parts.

Table 4. Positioning of the thermocouples (TC) in the laminates.

TC #	Laminate thickness	In-plane distance from central point	Through thickness position
1	thick (35 mm)	0 (centre)	0 (mould contact)
2	thick (35 mm)	63 mm	0 (mould contact)
3	thick (35 mm)	under edge wedge	0 (mould contact)
4	thick (35 mm)	0 (centre)	14 mm
5	thick (35 mm)	0 (centre)	7 mm
6	thick (35 mm)	0 (centre)	21 mm
7	thick (35 mm)	0 (centre)	28 mm
8	thick (35 mm)	0 (centre)	35 (bag contact)
9	thick (35 mm)	edge (125 mm)	17.5 mm
10	thin (12 mm)	0 (centre)	3 mm
11	thin (12 mm)	0 (centre)	0 (mould contact)
12	thin (12 mm)	63 mm	0 (mould contact)
13	thin (12 mm)	0 (centre)	6 mm
14	thin (12 mm)	0 (centre)	9 mm
15	thin (12 mm)	0 (centre)	12 mm (bag contact)
16	thin (12 mm)	outside	outside

pre-consolidated plates is very intrusive as the thermocouple thickness prevents good stacking. Nonetheless once the stacking os fully molten, during the consolidation dwell, the theromcouples are fully nested in the laminates and intrusiveness is reduced.

The temperature and α fields are compared in two directions: the first following path A, as shown in Fig. 5, the second being the one described by the position of the TCKs located through the thickness

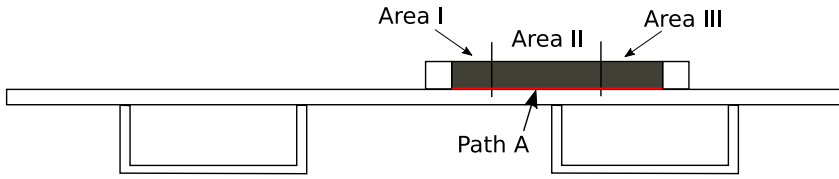

Figure 5. Experimental set-up and description of the three areas of interest and location of path A.

of the part. Fig. 5 also depicts the three areas of interest (denoted I, II and III) used in the analysis.

Below, a comparison between the experimental observations and numerical simulations is made to discuss the advantages and the limits of the models. Some experimental observations are then discussed.

Model validation

The experimental work was conducted in an oven with a temperature loading presented in Table 3. Thermal contact resistance (TCR) between the mold and the part is identified by TCK2 and TCK12. The convection coefficient is identified by TCK8 and the conductivity by TCK5, 6 and 7.

Fig. 6 shows the temperature differences between the experimental and numerical measurements. The relative error is plotted against time for six different thermocouples. Two fairly distinct phases can be seen:

- Between 0 and 1.5 hours, there are significant discrepancies. This can mainly be explained by the size of the TCKs. Indeed, given the size of a ply (approximately 0.180 mm) the $0.2mm$ diameter TCKs are rather intrusive and therefore create a local TCR with a thick air gap. This air gap persists until the resin melts and the pressure induced by the vacuum bag takes effect and thus reduces the TCR generated by the TCK.
  The inclusions created by the TCK then impose a local variation in conductivity. From a numerical point of view, since the part is considered perfect (assumption ii), there is no local variation in thermal conductivity, so some differences between experimental and numerical approach may then occur.

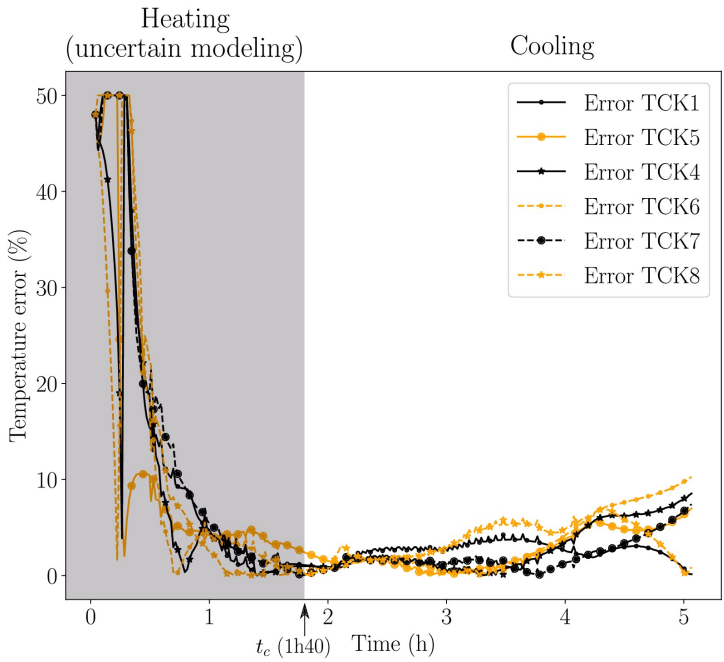

Figure 6. Relative error between measured and simulated temperatures plotted against time. The error is high during the heating phase and drops below 10% during the cooling phase.

This error decreases rather quickly to an error of about 5% after 1.5 hours. This is when the melting temperature of this material is reached. The resin thus becomes viscous and, combined with the applied pressure, the voids around each TCK collapse.
The same remarks can be made concerning the potential interply defects which create microporosities and thus micro TCR between each ply. This impacts the transverse conductivity and disturbs the thermal gradient. For the same reasons already mentioned, this phenomenon disappears once the resin is melted.
Another explanation may arise from the fact that the temperature values are very low at the beginning of consolidation. Thus, a deviation of a few degrees is enough to generate a significant error, whereas, in the middle of the consolidation, an error of a few degrees is not significant.

Finally Table 3 shows that the heating rate is much higher than the cooling rate (ratio of three). This generates higher thermal gradients and can potentially amplify the errors, especially with a higher sensitivity to thermal inertia.

- From 1 h 30 to 5 h, the average error varies by around 5%. The hypothesis of homogenized thermal conductivity seems to be correct even if it can reach a limit for extremely thick composite material. The remaining dispersion can be explained by the fact that the parameter identification method was not done by an inverse approach but in a pragmatic way using the thermocouple measurements.

Note: Concerning the thin plate, the gaps between simulations and experiments follow the same trend. For clarity, these are not displayed in Fig. 6.

Experimental observations

The first interesting approach when consolidating thick composites concerns the influence of the thickness on the associated temperature gradient. Fig. 7 shows the normalized temperature profiles (experimental and numerical) for both a thin and a thick CFTP part at time t = 1.2 h (at waiting time).
Two main observations confirm the intuitive effects during the consolidation of thick CFTP composite:

- First, the temperature gradient through the thickness is not linear for a thick part and is very steep during the heating stage (up to 125°C). Even the temperature on the lower side of the plate, which is in contact with the mold, evolves faster than the centre of the plate. This steep temperature gradient will induce high crystallization heterogeneity and, from a mechanical point of view, residual stresses. On the contrary, the gradient in the thin plate is shallower (up to 15°C). This leads to homogeneous crystallization and then a better consolidation quality of the final part.
- Second, the thermal inertia associated with the thickness of the thick CFTP part induces a temperature offset (both for heating and cooling phases) compared with the thin plate. This therefore implies large changes in consolidation times and cycles.

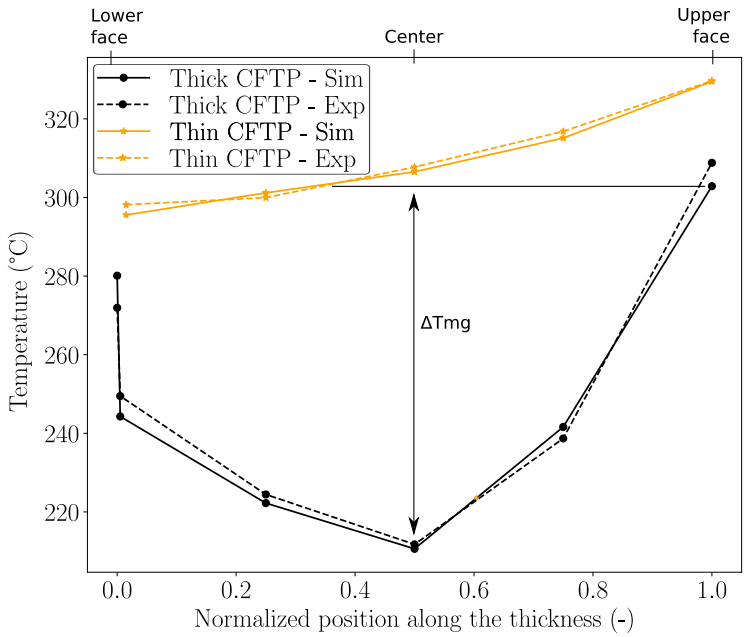

Figure 7. Normalized temperature profiles in thin and thick CFTP parts at the end of the heating stage ($t = 1.2$ h). Comparison with the simulation results. Temperature differences between core and skin are greater in thick parts.

It is also possible to see that the experimental results agree well with those from the numerical approach, despite the major assumptions (i, ii and iii). It is important to note that the differences are smaller for a thin plate than for a thick part. This can be explained by assumption (i), which stipulates that the material conductivity is supposed to be isotropic transverse and homogeneous. This assumption, already made for a thin part, can also be made for thick composite up to a critical thickness. Indeed, the more plies there are, the more defects the process will accumulate and the more false the assumption of the material being homogeneous will become (ii), which therefore impacts the thermal conductivity tensor.

In order to go further in the analysis of the temperature profile through the thickness, it is possible to calculate the difference between the point on the surface (TCK8 - TCK15) and the point in the centre of the part (TCK6 - TCK13). This difference, denoted $\Delta T_{mg}(t)$

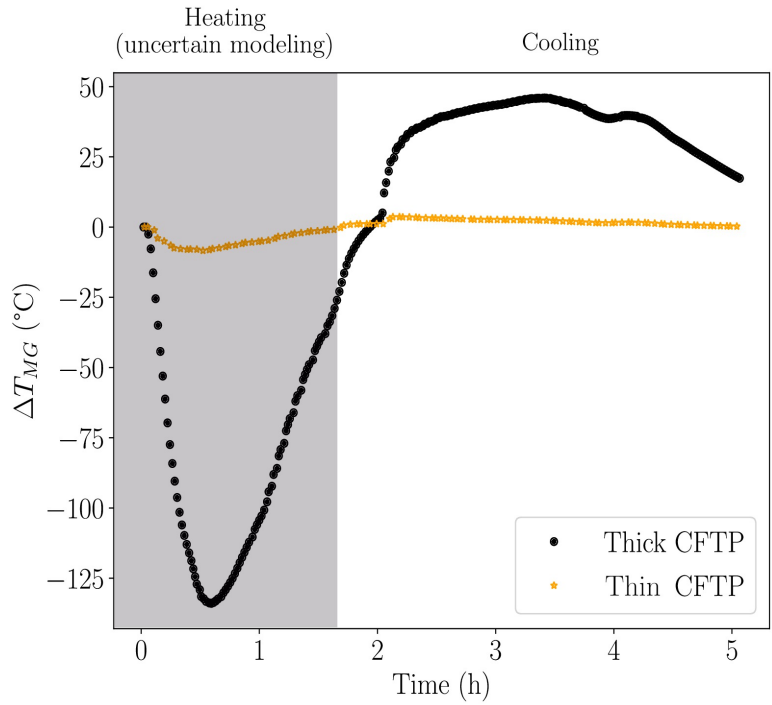

Figure 8. Temporal evolution of the difference between the highest and the lowest temperature for each part.

is shown as a function of time in Fig. 8. Significant temperature variations can appear that induce a more complex mechanical behaviour of the composite, since a mixture of solid and viscous phases must coexist.

Moreover, the variations in the thin plate are rather small and the gradient shape through its thickness is close to linear (rather than quadratic as can be seen in the thick part). As a result, the phase transition of the resin (whether solid to viscous or viscous to solid) is better controlled, the generation of stresses related to its crystallization is, therefore, reduced and the geometrical distortions are smaller.

Another interesting point is the dwell imposed during the thermal loading to reduce the temperature difference through the thickness. Indeed, for a thin plate, just a few minutes are enough to get the

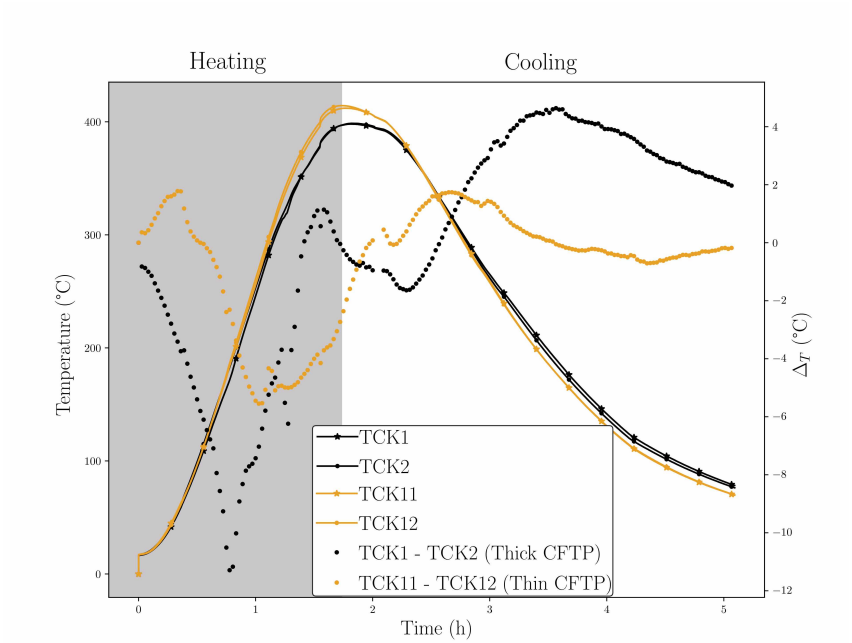

Figure 9. Experimental temperature differences between four TCKs located on path A.

plate completely melted. Nevertheless, it is possible to see in Fig. 8 that in the case of the thick plate, a difference of over 15°C remains, even at the end of the dwell. This is important because it shows that a longer waiting time is necessary. However, since the resin close to the surfaces is already above the melting temperature, it could be degraded and aging phenomena may impact the quality of the part.

A second interesting experimental observation concerns the temperature variations according to the geometry of the mold. Two TCKs were carefully placed between the part and the mold. One facing a support for each part (TCK2 and TC12 in Fig. 4), another one at a location without a support (TCK1 and TCK11 in Fig. 4). The goal was to compare the temperatures at these two specific locations, depending on the thickness of the CFTP parts, and to evaluate the thermal fin effect of the support.

Fig. 9 shows the differences between the two positions. Even though they are small for thin plates, they are much greater for thick composites. Thus, a temperature difference appears both in

the thickness and in the surface in contact with the mold. This, will generate a local variation on the crystallization field, potentially rendering the consolidation process non homogeneous.
In section *Complex geometry*, additional details will be provided on the impact of mold geometry on thick composite consolidation with a more complex case than a laboratory test.

Numerical analysis

Now we have seen that the experimental observations and experiment/simulation comparison show that the numerical approach is consistent, it is possible to run parametric studies using the numerical simulation. First, the influence of the mold geometry will be studied. Second, it will be shown that TCR is of major importance for the consolidation of a thick CFTP part. Finally, an example will be presented featuring complex industrial geometry.

Influence of mold geometry

Simulation results on mold geometry and the influence of the support on thick composite thermoplastic material are shown in Fig. 10, illustrating the temperature profile along path A (described in Fig. 5) for both thick and thin plates at time t = 3.1 h, during the cooling phase.

First, in relation to the previous section, it can be seen that the simulation is close to the experimental measurements (judging by TCK 1, 2, 11 and 12).

Second, unlike with the thin plate, distinct zones appear in the thick plate profile. Edge effects from the edge wedges are very important and are located in zones 1 and 3. In the second zone, the temperature variation is mainly due to the presence of the mold support. This thermal effect cannot be ignored and influences the consolidation process. The induced crystallization will itself be heterogeneous and thus the residual stresses on the part are not homogeneous. On a larger scale, this can have an impact on geometric distortions and microporosities.

Finally, in order to study the influence of the support on the temperature in detail, the quantity $\Delta T_m(t)$ is defined as the difference between $T_{p-approx}$ (see Fig. 10) and the temperature facing the

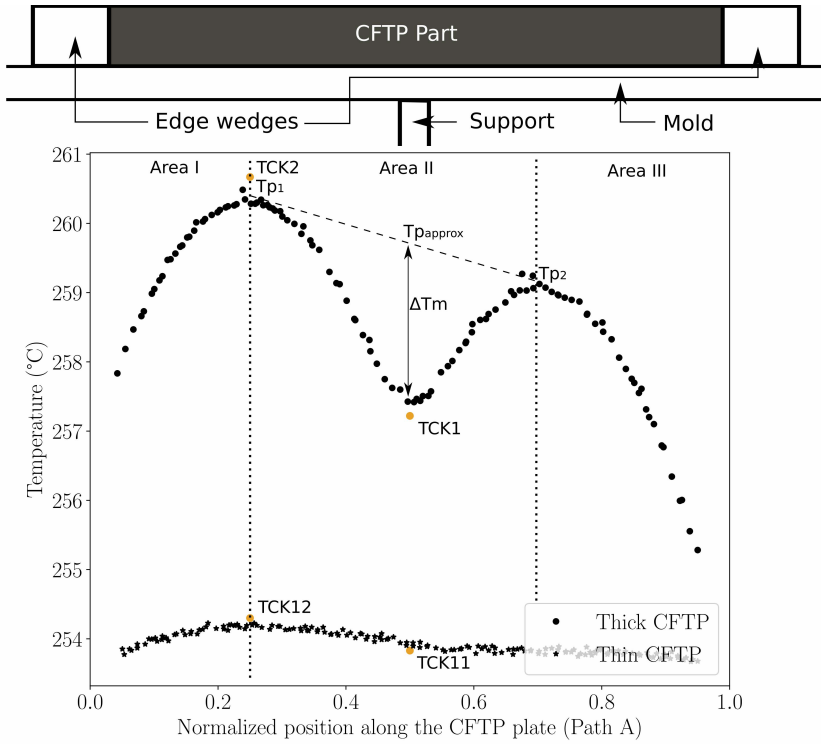

Figure 10. Shape of the temperature gradient along path A for both thin and thick CFTP parts at t = 3.1 h (cooling phase).

support. $T_{p-approx}$ is calculated by a linear interpolation between the temperature peaks (Tp1 and Tp2 in Fig. 10). $\Delta T_m(t)$ is then plotted as a function of time in Fig. 11.

Even if the temperature difference is small, it creates an offset in the degree of crystallization. In fact, the associated mechanism of crystallization is very sensitive to temperature and very rapid[76,77], meaning that just a few degrees of difference leads to an offset of the crystallization.

The shape of the crystallization field illustrated in Fig. 12 and the one induced by the steep thermal gradient through the thickness leads to the creation of a biphasic materal: generally melted but locally solid. This will result in heterogeneity of thermal and chemical shrinkages. These shrinkages will then create large geometrical

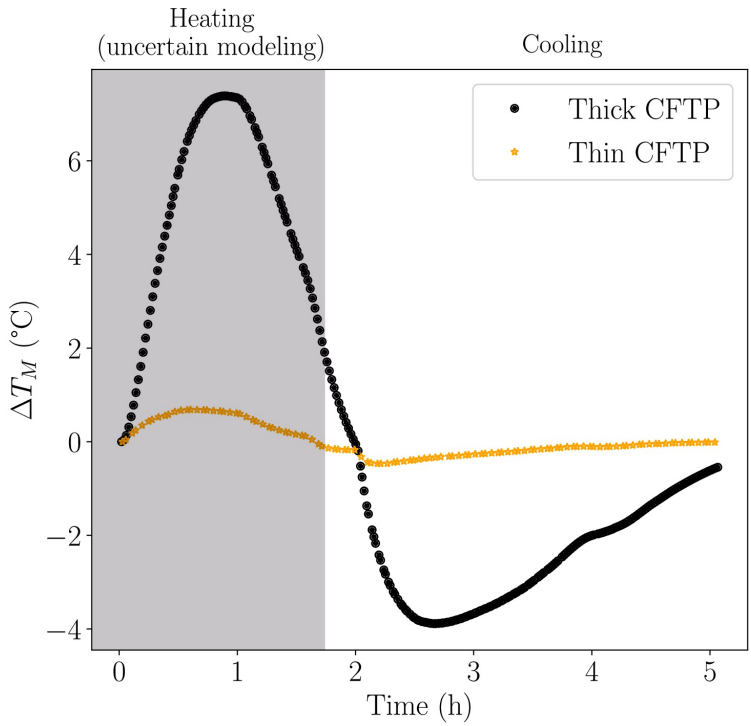

Figure 11. Temporal evolution of the temperature difference in the location above the support of the mold.

distortions and then residual stresses. The consolidation process is thus poorly controlled and the quality of the consolidated part can be affected.

In order to assess the influence of mold geometry in greater detail, a numerical analysis was made of the heat fluxes. Fig. 13 shows that the support has a significant impact on the heat flow. It ultimately plays the role of a thermal fin given its thickness (approximately 8 mm) compared with the thickness of the composite part. Two conclusions can be made based on the experimental and numerical observations:

- (i) Concerning the consolidation of a thin part: the thermal field is mainly ruled by the forced convection on the surface and by the transverse conductivity of the material.

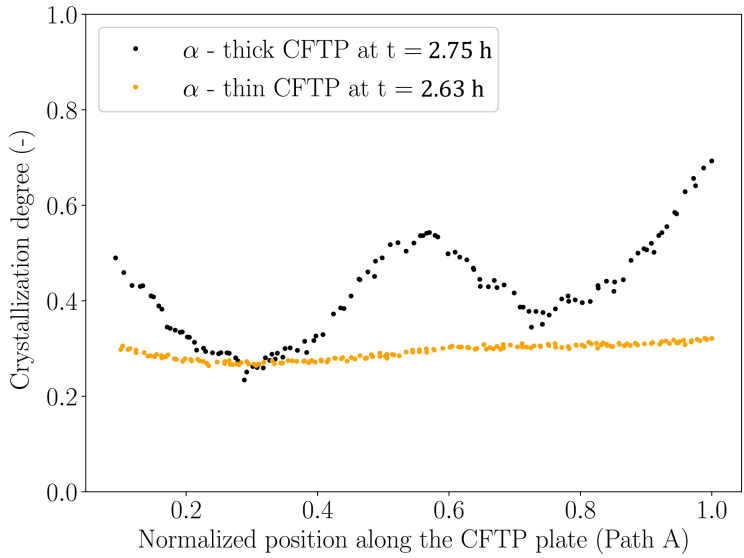

Figure 12. Influence of the support on the crystallization field shape. Impact on a thin and thick CFTP parts.

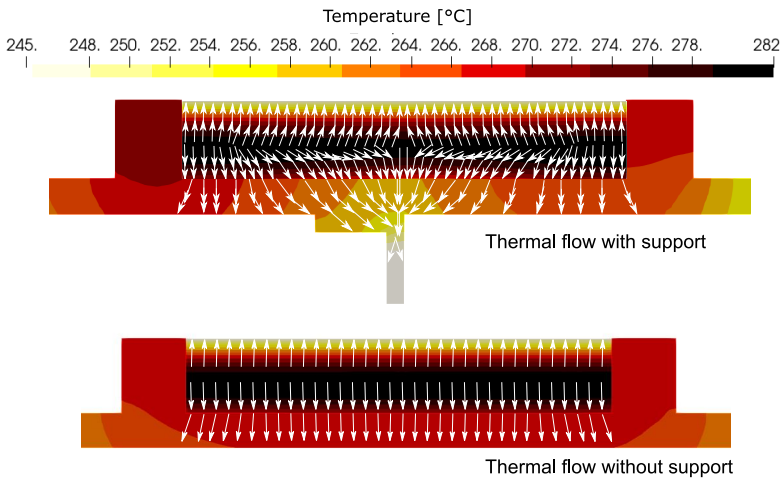

Figure 13. Graphical interpretation of the influence of the support of the mold on thermal flux. The arrows represent the heat fluxes.

- (ii) For a thick composite part: the thermal field is much more sensitive to many other parameters. The forced convection and

the transverse conductivity are important, but do not rule the thermal evolution in the part. It is important to take into account the geometry of the mold, the TCRs and the consolidation cycle. Edge effects, from the edge wedges, are also shown to be very important and must be considered.

From a physical point of view, it is possible to calculate the following dimensionless number (for an anisotropic transverse material):

$$\frac{\lambda_{plane}}{\lambda_{thickness}} \cdot \left(\frac{L_{thickness}}{L_{plane}} \right)^2 = N \tag{15}$$

where λ_{plane} is the conductivity in the plane of the CFTP part, $\lambda_{thickness}$ the transverse conductivity of the composite, L_{plane} the length of path A (see Fig. 5) and $L_{thickness}$ the thickness of the part.

If

$$N << 1 \tag{16}$$

Heat transfer is ruled by through-thickness conduction. However, if N is large, the in-plane conductivity needs to be considered in the heat transfer.

In this study:

$$\begin{cases} N_{12} = \frac{\lambda_{plane}}{\lambda_{thickness}} \cdot \left(\frac{250}{12}\right)^2 \approx 0.02 << 1 & \text{for a 12 mm thick CFTP} \\ N_{35} = \frac{\lambda_{plane}}{\lambda_{thickness}} \cdot \left(\frac{250}{35}\right)^2 \approx 0.2 \approx 1 & \text{for a 35 mm thick CFTP} \end{cases} \tag{17}$$

This confirms the numerical and experimental observations explained previously, notably concerning the temperature profile in Fig. 10.

Influence of thermal contact resistance

A second effect, often neglected in the case of thin plate, is the thermal contact resistance (TCR). A sensitivity study was conducted by running two simulations, modifying the TCR value TCR_0 by a value of δTCR. The reduced sensitivity RS is the sensitivity S divided by the reference value TCR_0:

$$\begin{cases} S = \frac{T_{TCR_0+\delta TCR} - T_{TCR_0}}{\delta TCR} \\ RS = \frac{1}{TCR_0} \cdot \frac{T_{TCR_0+\delta TCR} - T_{TCR_0}}{\delta TCR} \end{cases} \tag{18}$$

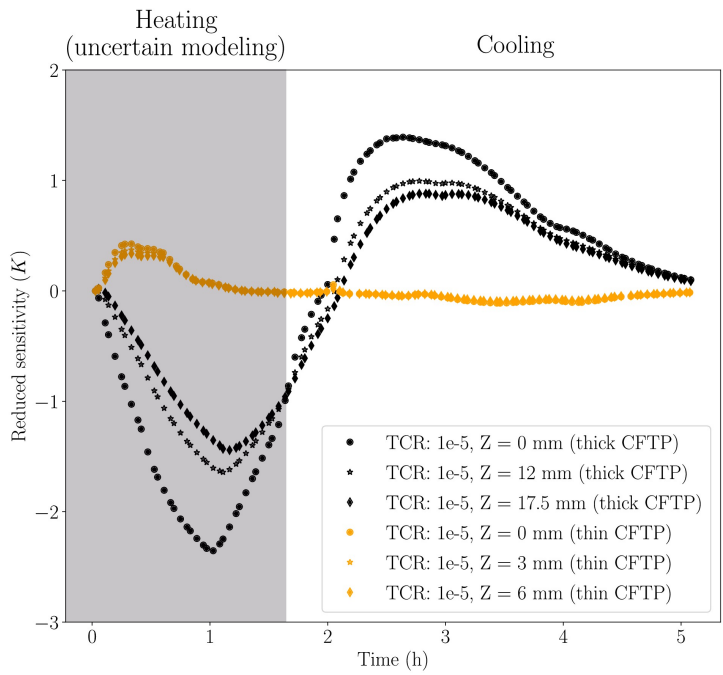

Figure 14. Reduced sensitivity to TCR for thick and thin composite parts at different depths through the thickness. The sensitivities are calculated from points in the middle of the part ($x = 125$ mm and $y = 125$ mm) and at different heights.

As can be seen in Fig. 14, for a thin plate, the reduced sensitivity to the TCR is rather small. On the contrary, for a thick plate, the reduced sensitivity to TCR is very high for both heating and cooling phases.

Fig. 14 also shows that the TCR sensitivity is very high for a thick part. This means that the slightest loss of contact between the part and the mold will have an important influence on the temperature field. To consider this contact loss, it is important to treat the evolution of TCR numerically on both temporal and spatial scales in the finite element calculation.

Moreover, by comparing different locations through the thickness, it is possible to notice that an offset is created. The TCR has an influence even in the core of the part.

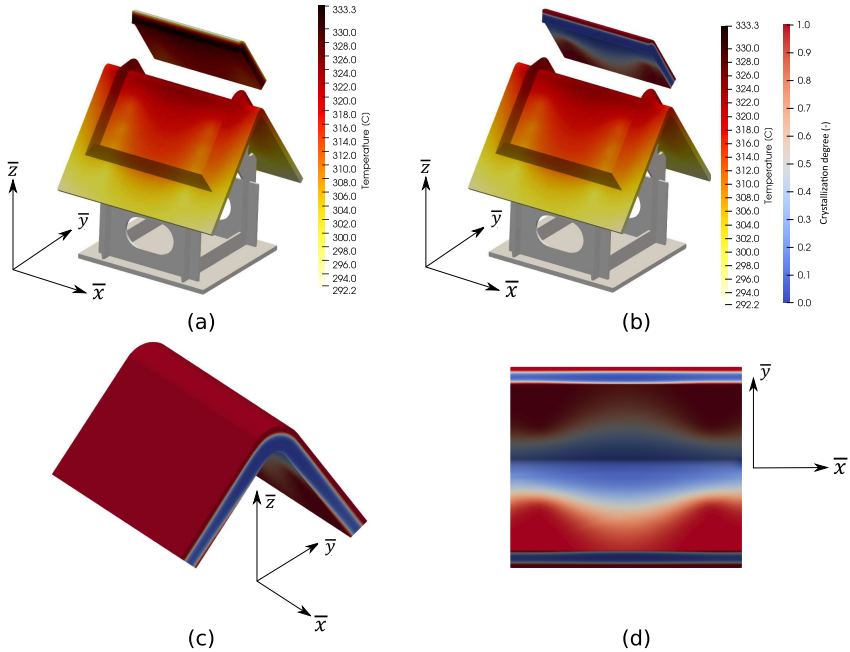

Figure 15. An example of complex geometry with support and angular forms (at t = 2.7 h): (a–b) thermal fields for the mold and half part, (c–d) crystallization degree field for the entire CFTP part.

Complex geometry

This section presents an analysis of the temperature field obtained for a complex industrial mold geometry designed for a corner (or bending plate) as shown in Fig. 15.

For such complex geometry, the phenomena previously described for a plate are amplified. It has previously been shown that the geometry of the mold has a strong influence on the temperature field. In the case of a corner, two phenomena will have an impact on the material health of the part once it is consolidated.

- (i): The temperature field and, therefore, crystallization field are not at all homogeneous, either along the surface between the mold and the part or through its thickness. This irregularity will induce residual stresses and localized geometrical distortions, thus potentially invalidating the material health and geometrical tolerances.

Moreover, since the shrinkage is localized and does not evolve in a homogeneous and controlled manner, the effects accumulate. In the case of the set-up of Fig. 15 (a), it was experimentally observed that the part tightens on the mold during cooling. This induces a movement of the part in the z direction and a loss of contact at the internal radius (see Fig. 15 (d)). Given the sensitivity to TCRs, the numerical and physical consideration of this parameter is important in this case.

- (ii): At a given time (t = 2.7 h), it is possible to see that a fully crystallized upper layer has formed, while the area near the inner radius is still in a molten state.
  This introduces serious problems for a good consolidation in the oven. Indeed, as can be seen in Fig. 15 (c), a solid upper layer is created on the entire upper face of the part while a large area of the part is still in a molten state. This solid layer on the surface of the part will redirect the pressure applied by the vacuum bag to the edge wedges, similarly to a keystone effect. This means that the area still in the molten state is no longer subject to pressure and local porosities will be created during crystallization. This was observed experimentally (see Fig. 16 (b)).

This test case shows that oven consolidation of thick parts with curved geometries is rather complex compared with the consolidation of thin parts. New phenomena have to be taken into account:

- (i): Consideration of the thermal impact of the mold from the design phase in order to minimize thermal effects harmful to the creation of homogeneous temperature and crystallization fields.
- (ii): Consideration of a temporally and spatially evolving contact resistance. Usually, TCR is considered constant and homogeneous and is used as a parameter to correct thermokinetic models.
- (iii): The imposed temperature cycles must also be studied and optimized in order to reduce temperature gradients, and thus crystallization, as much as possible.
- (iv): The geometry of the part must also be checked as significant shrinkage and stress effects may occur, such as keystone effects, local contact losses or warping.

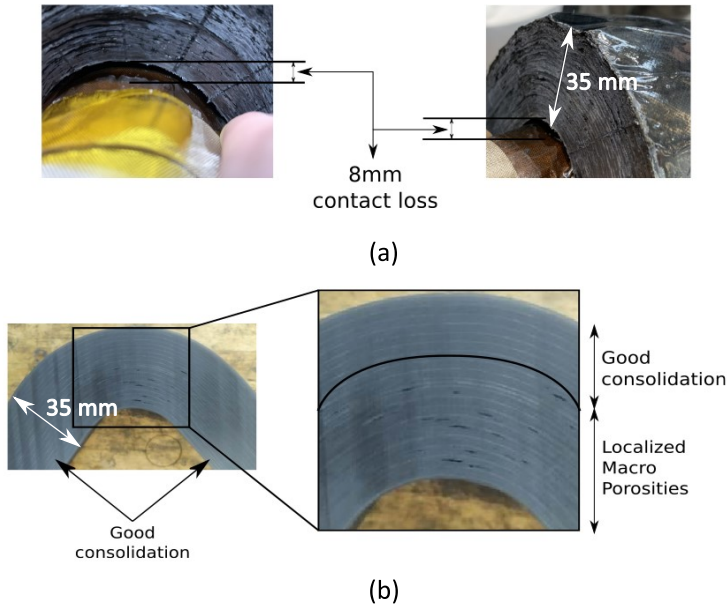

Figure 16. Experimental observations on a corner set-up: (a) gap caused by contact loss, (b) location of macro/microporosities in the bottom half of the thickness.

Conclusion

Through this paper, several experimental and numerical observations allowed us to highlight new phenomena during the consolidation of thick parts.

First, the major hypotheses were reviewed. It is possible to establish certain limits of validity. For example, the hypothesis (i) of homogeneous material works in the case of thick composite but it was shown that the transverse conductivity can be impacted due to defects and micro TCR between each ply. In the same way, the assumption of a perfectly draped part (ii, iii) is valid but requires precautions to be taken.

Second, new consideration is needed about the consolidation of thick parts. Indeed, it is usual to consider TCR as a constant to calibrate models for thin parts. In the case of thick composites, the sensitivity of the TCR is high, so it can no longer be considered as constant and homogeneous. In the same way, the geometry of the mold induces

variations in the temperature field and creates offsets in the degree of crystallization.

Third, the thermal cycle imposed in the oven must be adapted. Indeed, a cycle that is too slow to reduce the temperature gradients will degrade the resin. On the contrary, a cycle that is too fast will generate steep temperature gradients, consequent strong crystallization gradients and, therefore, residual stress, geometrical distortions and potential defects (porosities, etc.).

Finally, to be able to maintain the manufacturing reliability of the oven consolidation process, numerical simulation models must be able to consider all these details, particularly the scalable TCR.

To properly consider the contact loss and the shrinkages, it is important to incorporate the mechanical approaches into the modelling strategy presented here. This is subject to further work: development of a thermo-crystallo-mechanical analysis. Indeed, now that thermokinetic modelling has been applied, identified and validated, it is necessary to go further by being able to simulate the geometrical distortions and residual stresses.

Acknowledgements

The authors would like to acknowledge the funding they received from the MATCH program managed by IRT Jules Verne (French Institute for Research and Technology in Advanced Manufacturing Technologies for Composite, Metallic and Hybrid Structures). The authors wish to acknowledge the industrial and academic partners of this project: AIRBUS, LOIRETECH, DAHER, LS2N, ENSAM and LTeN laboratory. The authors would like to thank Vincent Sobotka at the University of Nantes without whom this study would not have been initiated.

References

1. Dufour C, Wang P, Boussu F et al. Experimental Investigation About Stamping Behaviour of 3D Warp Interlock Composite Preforms. *Applied Composite Materials* 2014; 21(5): 725–738.
2. De Luycker E, Morestin F, Boisse P et al. Simulation of 3D interlock composite preforming. *Composite Structures* 2009; 88(4): 615–623.
3. Badel P, Vidal-Salle E, Maire E et al. Simulation and tomography analysis of textile composite reinforcement deformation at the mesoscopic scale. *Deformation and Fracture of Composites: Analytical, Numerical and Experimental Techniques, with regular papers* 2008; 68(12): 2433–2440.

4. Zimmermann K, Zenkert D and Siemetzki M. Testing and analysis of ultra thick composites. *Composites Part B: Engineering* 2010; 41(4): 326–336. DOI:https://doi.org/10.1016/j.compositesb.2009.12.004. URL `https://www.sciencedirect.com/science/article/pii/S1359836809002200`.
5. Besson JM, Celli MA and Capelle N. Development of a carbon thermoplastic hub for the h160 helicopter. *JEC Composites magazine* 2017; 116.
6. Belnoue JPH, Nixon-Pearson OJ, Thompson AJ et al. Consolidation-Driven Defect Generation in Thick Composite Parts. *Journal of Manufacturing Science and Engineering* 2018; 140(7): 071006.
7. Saouab A, Bréard J, Lory P et al. Injection simulations of thick composite parts manufactured by the RTM process. *Composites Science and Technology* 2001; 61(3): 445–451.
8. Sorrentino L, Polini W and Bellini C. To design the cure process of thick composite parts: experimental and numerical results. *Advanced Composite Materials* 2014; 23(3): 225–238.
9. Ruiz E and Trochu F. Numerical analysis of cure temperature and internal stresses in thin and thick RTM parts. *Composites Part A: Applied Science and Manufacturing* 2005; 36(6): 806–826.
10. Gayot SF, Bailly C, Pardoen T et al. Processing maps based on polymerization modelling of thick methacrylic laminates. *Materials & Design* 2020; 196: 109170.
11. Hassan MH, Othman AR and Kamaruddin S. A review on the manufacturing defects of complex-shaped laminate in aircraft composite structures. *The International Journal of Advanced Manufacturing Technology* 2017; 91(9): 4081–4094.
12. Lawrence JM, Hsiao KT, Don RC et al. An approach to couple mold design and on-line control to manufacture complex composite parts by resin transfer molding. *Composites Part A: Applied Science and Manufacturing* 2002; 33(7): 981–990.
13. Wang X, Zhang Z, Xie F et al. Correlated rules between complex structure of composite components and manufacturing defects in autoclave molding technology. *Journal of reinforced plastics and composites* 2009; 28(22): 2791–2803.
14. Xin C, Gu Y, Li M et al. Experimental and numerical study on the effect of rubber mold configuration on the compaction of composite angle laminates during autoclave processing. *Composites Part A: Applied Science and Manufacturing* 2011; 42(10): 1353–1360. DOI:https://doi.org/10.1016/j.compositesa.2011.05.018. URL `https://www.sciencedirect.com/science/article/pii/S1359835X11001709`.
15. Parlevliet PP, Bersee HE and Beukers A. Residual stresses in thermoplastic composites?A study of the literature?Part I: Formation of residual stresses. *Composites Part A: Applied Science and Manufacturing* 2006; 37(11): 1847–1857. Publisher: Elsevier.
16. Menna C, Asprone D, Caprino G et al. Numerical simulation of impact tests on gfrp composite laminates. *International Journal of Impact Engineering* 2011; 38(8): 677–685. DOI:https://doi.org/10.1016/j.ijimpeng.2011.03.003. URL `https://www.sciencedirect.com/science/article/pii/S0734743X1100056X`.
17. Parlevliet PP. *Residual strains in thick thermoplastic composites: an experimental approach*. PhD Thesis, Delft University of Technology, 2010.

18. Netzel C, Mordasini A, Schubert J et al. An experimental study of defect evolution in corners by autoclave processing of prepreg material. *Composites Part A: Applied Science and Manufacturing* 2021; 144: 106348. DOI:https://doi.org/10.1016/j.compositesa.2021.106348. URL `https://www.sciencedirect.com/science/article/pii/S1359835X21000737`.
19. Kobayashi S, Tsukada T and Morimoto T. Resin impregnation behavior in carbon fiber reinforced polyamide 6 composite: Effects of yarn thickness, fabric lamination and sizing agent. *Composites Part A: Applied Science and Manufacturing* 2017; 101: 283–289.
20. Tsukada T, Minakuchi S and Takeda N. Identification of process-induced residual stress/strain distribution in thick thermoplastic composites based on in situ strain monitoring using optical fiber sensors. *Journal of Composite Materials* 2019; 53(24): 3445–3458.
21. Zhu F, Gong Y, Bai P et al. High-accuracy biaxial optical extensometer based on 2D digital image correlation. *Measurement Science and Technology* 2017; 28(8): 085006.
22. Bogetti TA and Gillespie JW. Two-Dimensional Cure Simulation of Thick Thermosetting Composites. *Journal of Composite Materials* 1991; : 35.
23. Nakouzi S, Pancrace J, Schmidt FM et al. Curing Simulation of Composites Coupled with Infrared Heating. *International Journal of Material Forming* 2010; 3(S1): 587–590.
24. Nakouzi S, Berthet F, Le Maoult Y et al. Simulations of an Infrared Composite Curing Process. *Key Engineering Materials* 2013; 554-557: 1517–1522.
25. White S and Hahn H. Process Modeling of Composite Materials: Residual Stress Development during Cure. Part II. Experimental Validation. *Journal of Composite Materials* 1992; 26(16): 2423–2453.
26. Lu S, Chen D, Wang X et al. Real-time cure behaviour monitoring of polymer composites using a highly flexible and sensitive CNT buckypaper sensor. *Composites Science and Technology* 2017; 152: 181–189.
27. Silikas N, Eliades G and Watts D. Light intensity effects on resin-composite degree of conversion and shrinkage strain. *Dental Materials* 2000; 16(4): 292–296.
28. Wisnom M, Gigliotti M, Ersoy N et al. Mechanisms generating residual stresses and distortion during manufacture of polymer-matrix composite structures. *Composites Part A: Applied Science and Manufacturing* 2006; 37(4): 522–529.
29. Rouison D, Sain M and Couturier M. Resin transfer molding of natural fiber reinforced composites: cure simulation. *Composites Science and Technology* 2004; 64(5): 629–644.
30. Teplinsky S and Gutman E. Computer simulation of process induced stress and strain development during cure of thick-section thermosetting composites. *Computational Materials Science* 1996; 6(1): 71–76.
31. Ali M, Nawab Y, Saouab A et al. Fabrication induced spring-back in thermosetting woven composite parts with variable thickness. *Journal of Industrial Textiles* 2018; 47(6): 1291–1304.
32. Ersoy N, Potter K, Wisnom MR et al. Development of spring-in angle during cure of a thermosetting composite. *Composites Part A: Applied Science and Manufacturing*

2005; 36(12): 1700–1706.
33. Hojjati M and Hoa S. Curing simulation of thick thermosetting composites. *Composites Manufacturing* 1994; 5(3): 159–169. Publisher: Elsevier.
34. Zhu Q, Geubelle PH, Li M et al. Dimensional Accuracy of Thermoset Composites: Simulation of Process-Induced Residual Stresses. *Journal of Composite Materials* 2001; 35(24): 2171–2205.
35. Kravchenko OG, Kravchenko SG and Pipes RB. Chemical and thermal shrinkage in thermosetting prepreg. *Composites Part A: Applied Science and Manufacturing* 2016; 80: 72–81.
36. Kravchenko OG, Li C, Strachan A et al. Prediction of the chemical and thermal shrinkage in a thermoset polymer. *Composites Part A: Applied Science and Manufacturing* 2014; 66: 35–43.
37. Nawab Y, Park CH, Saouab A et al. Modeling the residual stress in woven thermoset composites parts for aerospace applications using finite element methods. In *Advanced Materials Research*, volume 1099. Trans Tech Publ, pp. 32–36.
38. Nawab Y and Jacquemin F. From the Characterization and Modeling of Cure-Dependent Properties of Composite Materials to the Simulation of Residual Stresses. *Heat transfer in polymer composite materials: Forming processes* 2016; : 157–174.
39. Singer G, Sinn G, Lichtenegger HC et al. Evaluation of in-situ shrinkage and expansion properties of polymer composite materials for adhesive anchor systems by a novel approach based on digital image correlation. *Polymer Testing* 2019; 79: 106035. Publisher: Elsevier.
40. Danielson C, Mehrnezhad A, YekrangSafakar A et al. Fabrication and characterization of self-folding thermoplastic sheets using unbalanced thermal shrinkage. *Soft Matter* 2017; 13(23): 4224–4230. Publisher: Royal Society of Chemistry.
41. Di Landro L and Pegoraro M. Carbon fibre thermoplastic matrix adhesion. *Journal of Materials Science* 1987; 22(6): 1980–1986. Publisher: Springer.
42. Li D, Li X, Dai J et al. A Comparison of Curing Process-Induced Residual Stresses and Cure Shrinkage in Micro-Scale Composite Structures with Different Constitutive Laws. *Applied Composite Materials* 2018; 25(1): 67–84.
43. Rashidi A, Belnoue JPH, Thompson AJ et al. Consolidation-driven wrinkling in carbon/epoxy woven fabric prepregs: An experimental and numerical study. *Composites Part A: Applied Science and Manufacturing* 2021; 143: 106298.
44. Kaminski GEC Deborah A, Center D and Kaminski DA. *Heat transfer data book*. Schenectady, N.Y. : General Electric Company Corporate Research and Development, 1977. Type: Book; Book/Illustrated.
45. Domingues G, Rochais D and Volz S. Thermal contact resistance between two nanoparticles. *Journal of computational and theoretical nanoscience* 2008; 5(2): 153–156.
46. Somé SC, Delaunay D, Faraj J et al. Modeling of the thermal contact resistance time evolution at polymer–mold interface during injection molding: Effect of polymers' solidification. *Applied Thermal Engineering* 2015; 84: 150–157.

47. Somé SC, Delaunay D and Gaudefroy V. Comparison and validation of thermal contact resistance models at solid–liquid interface taking into account the wettability parameters. *Applied thermal engineering* 2013; 61(2): 531–540.
48. Nakamura K, Watanabe T, Katayama K et al. Some aspects of nonisothermal crystallization of polymers. I. Relationship between crystallization temperature, crystallinity, and cooling conditions. *Journal of Applied Polymer Science* 1972; 16(5): 1077–1091.
49. Tardif X, Pignon B, Boyard N et al. Experimental study of crystallization of polyetheretherketone (peek) over a large temperature range using a nano-calorimeter. *Polymer Testing* 2014; 36: 10–19.
50. Landry B and Hubert P. Experimental study of defect formation during processing of randomly-oriented strand carbon/peek composites. *Composites Part A: Applied Science and Manufacturing* 2015; 77: 301–309.
51. Holmes ST and Gillespie Jr JW. Thermal analysis for resistance welding of large-scale thermoplastic composite joints. *Journal of Reinforced Plastics and Composites* 1993; 12(6): 723–736.
52. Choupin T, Fayolle B, Régnier G et al. A more reliable dsc-based methodology to study crystallization kinetics: Application to poly (ether ketone ketone)(pekk) copolymers. *Polymer* 2018; 155: 109–115.
53. Cogswell FN. *Thermoplastic aromatic polymer composites: a study of the structure, processing and properties of carbon fibre reinforced polyetheretherketone and related materials*. Elsevier, 2013.
54. Lamèthe JF. *Etude de l'adhésion de composites thermoplastiques semi-cristallins; application à la mise en oeuvre par soudure*. PhD Thesis, Université Pierre et Marie Curie-Paris VI, 2004.
55. Hecht F. New development in freefem++. *J Numer Math* 2012; 20(3-4): 251–265. URL `https://freefem.org/`.
56. Castell A, Solé C, Medrano M et al. Natural convection heat transfer coefficients in phase change material (pcm) modules with external vertical fins. *Applied thermal engineering* 2008; 28(13): 1676–1686.
57. Baumard T, De Almeida O, Menary G et al. Determination of thermal contact conductance in vacuum-bagged thermoplastic prepreg stacks using infrared thermography. In *AIP Conference Proceedings*. AIP Publishing LLC, p. 110002.
58. Research GEC, Center D and Kaminski DA. *Heat Transfer Data Book*. General Electric Company Corporate Research and Development, 1977.
59. Lecointe D. *Caractérisation et simulation des processus de transferts lors d'injection de résine pour le procédé RTM*. PhD Thesis, Université de Nantes, 1999.
60. Levy A, Le Corre S and Sobotka V. Heat transfer and crystallization kinetics in thermoplastic composite processing. A coupled modelling framework. In *AIP Conference Proceedings*, volume 1769. AIP Publishing, p. 170038.
61. Castell A, Solé C, Medrano M et al. Natural convection heat transfer coefficients in phase change material (PCM) modules with external vertical fins. *Applied Thermal Engineering* 2008; 28(13): 1676–1686.
62. Hahn DW and Özisik MN. *Heat conduction*. John Wiley & Sons, 2012.

63. Bendada A, Derdouri A, Lamontagne M et al. Analysis of thermal contact resistance between polymer and mold in injection molding. *Applied Thermal Engineering* 2004; 24(14-15): 2029–2040.
64. Massé H, Arquis E, Delaunay D et al. Heat transfer with mechanically driven thermal contact resistance at the polymer?mold interface in injection molding of polymers. *International Journal of Heat and Mass Transfer* 2004; 47(8-9): 2015–2027.
65. Thomas T and Probert S. Thermal contact resistance: The directional effect and other problems. *International Journal of Heat and Mass Transfer* 1970; 13(5): 789–807.
66. Sridhar L and Narh KA. Measurement and Modeling of Thermal Contact Resistance at a Plastic-Metal Interface. In *APS March Meeting Abstracts*. pp. 2273–2277.
67. Salgon J, Robbe-Valloire F, Blouet J et al. A mechanical and geometrical approach to thermal contact resistance. *International Journal of Heat and Mass Transfer* 1997; 40(5): 1121–1129.
68. Hecht F. FreeFeml Documentation, Release 4.6, 2020.
69. Avrami M. Kinetics of phase change. I General theory. *The Journal of chemical physics* 1939; 7(12): 1103–1112. Publisher: American Institute of Physics.
70. Kawabata S. *The Standardization and Analysis of Hand Evaluation*. Textile Machinery Society of Japan, 1980.
71. Kawabata S, Niwa M and Kawai H. Finite-deformation theory of plain-weave fabrics - 3. The shear-deformation theory. *Journal of the Textile Institute* 1973; 64(2): 62–85.
72. Nakamura K, Watanabe T, Katayama K et al. Some aspects of nonisothermal crystallization of polymers. I. Relationship between crystallization temperature, crystallinity, and cooling conditions. *Journal of Applied Polymer Science* 1972; 16(5): 1077–1091. Publisher: Wiley Online Library.
73. Levy A. Robust Numerical Resolution of Nakamura Crystallization Kinetics. *International Journal of Theoretical and Applied Mathematics* 2017; 3(4): 143.
74. Tardif X, Pignon B, Boyard N et al. Experimental study of crystallization of PolyEtherEtherKetone (PEEK) over a large temperature range using a nano-calorimeter. *Polymer Testing* 2014; 36: 10–19. Publisher: Elsevier.
75. Ypma TJ. Historical development of the Newton?Raphson method. *SIAM review* 1995; 37(4): 531–551. Publisher: SIAM.
76. Levy A, Hoang DA and Le Corre S. On the Alternate Direction Implicit (ADI) Method for Solving Heat Transfer in Composite Stamping. *Materials Sciences and Applications* 2016; 8(1): 37–63. Publisher: Scientific Research Publishing.
77. Levy A, Le Corre S and Sobotka V. Heat transfer and crystallization kinetics in thermoplastic composite processing. A coupled modelling framework. In *AIP Conference Proceedings*, volume 1769. AIP Publishing, p. 170038.